*IEEE TRANSACTIONS ON POWER SYSTEMS*, VOL. 7, NO. 2, MAY 1992, PP. 673–683.

# POINT OF COLLAPSE METHODS APPLIED TO AC/DC POWER SYSTEMS

Claudio A. Cañizares, Student Member, IEEE
Fernando L. Alvarado, Senior Member, IEEE
Christopher L. DeMarco, Member, IEEE
Ian Dobson, Member, IEEE
Willis F. Long, Fellow, IEEE
University of Wisconsin–Madison
Madison, Wisconsin 53706 USA

Abstract: This paper describes an extension of the Point of Collapse method developed for ac systems studies to the determination of saddle-node bifurcations in power systems including high voltage direct current (HVDC) transmission. Bus voltage profiles are illustrated for an ac/dc test system, which significantly differ from the profiles of pure ac systems for typical system models. In particular, voltage dependent current order limits (VDCOLs) are shown to affect the voltage profiles ("nose" curves) and the loadability margin of the system. It is also shown that Hopf bifurcations, which are not possible in purely ac lossless systems with second-order generator models, become plausible when the dynamics for the HVDC system are included.

Keywords: Voltage collapse, HVDC, singularity, point of collapse, saddle-node bifurcations, Hopf bifurcations.

## INTRODUCTION

Voltage instability and collapse have been observed in several electric power networks throughout the world, and have been the subject of increasing study over the past few years [1]. Furthermore, the relative wide spread use of HVDC systems for the transmission of large amounts of power [2, 3, 4, 5] has motivated several researchers to study voltage stability issues in ac/dc systems by using voltage sensitivity factors (VSFs) [6, 7]. The VSF has been shown not to be a good measure of proximity to collapse in ac systems [1], especially for buses with large amounts of reactive support. This paper analyzes the problem using bifurcation theory of nonlinear systems to determine the distance in state space to the point of collapse, so that better estimates of the loadability margins of the ac/dc system can be obtained.

Here some of the mathematical and computational tools for voltage stability studies in ac systems are extended to incorporate HVDC models, and to gain new insight into the nature of the voltage collapse problem in ac/dc systems. Moreover, the paper discusses some of the difficulties encountered during the calculation of the unstable equilibrium points (i.e., additional solutions of the power flow equations corresponding to unstable eigenvalues of the linearized ac/dc system dynamic equations), which have proven useful in voltage stability analysis of ac systems [8, 9].

This paper is organized as follows. The assumptions and models representing the ac/dc system transient behavior are first presented. Next, the mathematical background describing bifurcation (voltage collapse) phenomena for the ac/dc system equations is discussed. Numerical techniques used to locate the loading levels that correspond to the bifurcation point are also described. Finally, these techniques are applied to a reduced ac/dc sample system.

## SYSTEM MODELS AND ASSUMPTIONS

The ac system is represented using transient stability models that assume quasi-static evolution of bus voltage phasors on the time scale of interest [5].

### Generators ($n_G$)

Voltage $V_g$ sources behind transient reactance $X'_d$ are used, and q-axis transient voltage dynamics are included. Generator $n_G$ is the system reference ($\delta_{n_G} = 0$).

$$\begin{aligned}
\dot{\delta}_g &= \omega_g - \omega_{n_G} \qquad (1)\\
\dot{\omega}_g &= \frac{1}{M_g}\left(P_m^0 - P_{gt} - D_g\omega_g\right)\\
\dot{V}_g &= \frac{X_d - X'_d}{T'_{d_o}}\left[\frac{E_f - V_g}{X_d - X'_d} - \frac{V_g}{X'_d} + \frac{V_t}{X'_d}\cos(\delta_t - \delta_g)\right]\\
P_{gt} &= \frac{V_g V_t}{X'_d}\sin(\delta_g - \delta_t)\\
Q_{gt} &= -\frac{V_t^2}{X'_d} + \frac{V_g V_t}{X'_d}\cos(\delta_g - \delta_t)
\end{aligned}$$

Here $P_{gt}$ and $Q_{gt}$ are the powers injected by the generator at bus $t$. $E_f$ represents the field voltage, and $X_d$ stands for the synchronous generator reactance. While $E_f$ is held constant in these equations, more detailed exciter dynamics can be easily added.

**Transmission System**

A constant admittance model ($G$, $B$, $B_s$) is employed.

$$\begin{aligned} P_{sr} &= GV_s^2 - GV_sV_r\cos(\delta_s-\delta_r) \\ &\quad + BV_sV_r\sin(\delta_s-\delta_r) \\ Q_{sr} &= (B_s+B)V_s^2 - GV_sV_r\sin(\delta_s-\delta_r) \\ &\quad - BV_sV_r\cos(\delta_s-\delta_r) \end{aligned} \tag{2}$$

Here $P_{sr}$ and $Q_{sr}$ are the transmitted powers from bus $s$ to bus $r$.

**Loads ($n_L$)**

Voltage and frequency dependent load models are employed.

$$\begin{aligned} P_l &= P_{l_1}\left(\frac{V_l}{V_l^0}\right)^2 + P_{l_2}\left(\frac{V_l}{V_l^0}\right) + P_{l_3} \\ &\quad + D_l(\dot{\delta}_l + \omega_{n_G}) + \lambda\Delta P_l \\ Q_l &= Q_{l_1}\left(\frac{V_l}{V_l^0}\right)^2 + Q_{l_2}\left(\frac{V_l}{V_l^0}\right) + Q_{l_3} + \lambda\Delta Q_l \end{aligned} \tag{3}$$

Here $P_l$ and $Q_l$ are the powers absorbed by the load at bus $l$, and $\lambda$ is a parameter used to simulate the slow time scale load variation that drives the system to collapse. $D_l$ is the load frequency coefficient (a time constant in seconds).

**HVDC ($n_{dc}$)**

A variation of typical control schemes is used to represent the HVDC converter behavior in quasi-static operation (Fig. 1). This scheme can be realized using the control circuit depicted in Fig. 2. Notice that the VDCOL is modelled as a nonlinear function of the converter ac bus voltage.

The HVDC link as represented here has basically two different control regimes. Under normal operating conditions, the rectifier controller controls the current while the inverter current controller remains saturated (and therefore "out of the loop"). However, when the system experiences a fault condition, the rectifier controller can be driven into saturation while the inverter controller "takes over" the current control. The HVDC system can be modelled, under normal operating conditions and assuming ideal harmonic filtering, by [2, 3, 4, 5]:

$$\begin{aligned} \dot{I}_d &= \frac{1}{L_d}(V_{d_r} - V_{d_i}) - \frac{R_d}{L_d}I_d \\ \dot{x}_r &= K_I[I_{o_r}(V_r) - I_d] \\ \cos\alpha_r &= x_r + K_P[I_{o_r}(V_r) - I_d] \\ V_{d_r} &= \frac{3\sqrt{2}}{\pi}a_rV_r\cos\alpha_r - \frac{3}{\pi}X_{c_r}I_d \\ S_r &= \frac{V_nI_n}{S_n}\frac{3\sqrt{2}}{\pi}a_rV_rI_d \\ P_r &= \frac{V_nI_n}{S_n}V_{d_r}I_d \end{aligned} \tag{4}$$

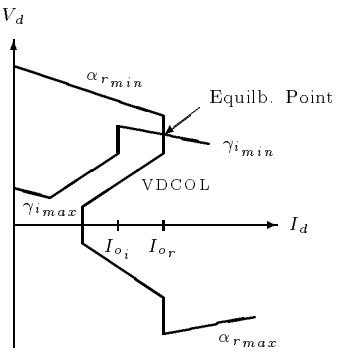


**Fig. 1**: *HVDC control criteria. Notice that the rectifier is allowed to go into inverter operation for faster recovery after fault conditions.*

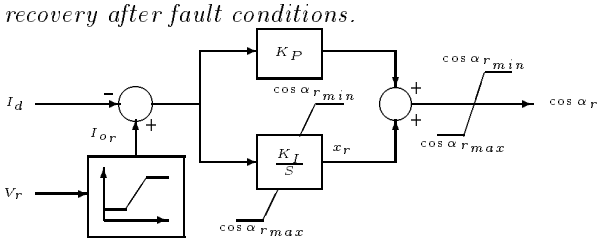


**Fig. 2**: *PI rectifier current controller. The inverter side has a similar control circuit.*

$$\begin{aligned} Q_r &= \sqrt{S_r^2 - P_r^2} \\ \cos\gamma_i &= \cos\gamma_{i_{min}} \\ V_{d_i} &= \frac{3\sqrt{2}}{\pi}a_iV_i\cos\gamma_i - \frac{3}{\pi}X_{c_i}I_d \\ S_i &= \frac{V_nI_n}{S_n}\frac{3\sqrt{2}}{\pi}a_iV_iI_d \\ P_i &= -\frac{V_nI_n}{S_n}V_{d_i}I_d \\ Q_i &= \sqrt{S_i^2 - P_i^2} \end{aligned}$$

Here $V_{d_r}$ and $V_{d_i}$ are the per unit dc terminal voltages at the rectifier and inverter ends, respectively. $I_n$ (kA) and $V_n$ (kV) are the base quantities for the dc system, and $S_n$ is the base power in MVA for the ac side. $X_{c_r}$ and $X_{c_i}$ are the per unit commutation reactances, and $R_d$ and $L_d$ are the per unit dc line parameters. The products $a_rV_r$ and $a_iV_i$ are the per unit ac bus voltages at the secondary side of the transformers with respect to the dc bus voltage base $V_n$. $S_r$ and $S_i$ are the per unit magnitudes of the HVDC complex powers at the ac side, and $P_r$, $P_i$, $Q_r$ and $Q_i$ are the per unit active and reactive powers absorbed by the dc system. When the inverter takes over current control, the equations for $\dot{x}_r$, $\cos\alpha_r$, and $\cos\gamma_i$ are replaced by:

$$\begin{aligned} \dot{x}_i &= K_I[I_d - I_{o_i}(V_i)] \\ \cos\gamma_i &= x_i + K_P[I_d - I_{o_i}(V_i)] \\ \cos\alpha_r &= \cos\alpha_{r_{min}} \end{aligned} \tag{5}$$

These equations are valid, within a roughly 4% er-

ror margin, for overlap angles $\mu_r$ and $\mu_i$ of up to $60^0$, i.e., there is a (three-valve) commutation every $60^0$ in a six-pulse bridge. They are not valid for four-valve commutation, since under these operating conditions the dc link must be represented by a different set of equations [5].

The controller model is such that inverter current control and rectifier current control typically do not overlap. For high rectifier voltages and/or low inverter voltages the rectifier current controller is in operation while the inverter controller is saturated at its minimum value $\gamma_{i_{min}}$; conversely, for low rectifier voltages and/or high inverter voltages the roles of inverter and rectifier controllers are reversed. During recovery from fault conditions it is typical to have both converters controlling the current for a brief period. Each one of these cases is represented by "switching" to the appropriate set of differential equations.

The following vectors are defined for rectifier current control at each HVDC link ($k = 1, 2, \cdots, n_{dc}$):

$$\begin{aligned}
\mathbf{x}_{dc_k} &= [x_{r_k}\ I_{d_k}]^T \\
\mathbf{y}_{dc_k} &= [\cos\alpha_{r_k}\ V_{d_{r_k}}\ S_{r_k}\ \cos\gamma_{i_k}\ V_{d_{i_k}}\ S_{i_k}]^T \\
\mathbf{V}_{dc_k} &= [V_{r_k}\ V_{i_k}]^T \\
\mathbf{P}_{dc_k} &= [P_{r_k}\ P_{i_k}]^T \\
\mathbf{Q}_{dc_k} &= [Q_{r_k}\ Q_{i_k}]^T
\end{aligned}$$

These vectors change when the inverter controls the dc current. In either case equations (4) can be rewritten as:

$$\begin{aligned}
\dot{\mathbf{x}}_{dc_k} &= \mathbf{h}_{dc_k}(\mathbf{V}_{dc_k}, \mathbf{x}_{dc_k}, \mathbf{y}_{dc_k}) \\
\mathbf{0} &= \mathbf{w}_{dc_k}(\mathbf{V}_{dc_k}, \mathbf{x}_{dc_k}, \mathbf{y}_{dc_k}) \\
\mathbf{P}_{dc_k} &= \mathbf{f}_k(\mathbf{V}_{dc_k}, \mathbf{x}_{dc_k}, \mathbf{y}_{dc_k}) \\
\mathbf{Q}_{dc_k} &= \mathbf{g}_k(\mathbf{V}_{dc_k}, \mathbf{x}_{dc_k}, \mathbf{y}_{dc_k})
\end{aligned} \tag{6}$$

## Vector Equations

Equations (1) to (5) can be arranged into vector differential equations (7) for an $n$ bus ac/dc system ($n = n_G + n_L + 2n_{dc}$). The vectors $\mathbf{f}(\cdot)$ and $\mathbf{g}(\cdot)$ stand for normalized ac active and reactive power flow mismatch equations, respectively, and $\mathbf{V} = [\mathbf{V}_G^T\ \mathbf{V}_L^T\ \mathbf{V}_{dc}^T]^T$ and $\boldsymbol{\delta} = [\boldsymbol{\delta}_G^T\ \boldsymbol{\delta}_L^T\ \boldsymbol{\delta}_{dc}^T]^T$. To simplify the eigenvalue analysis, the reference generator $n_G$ is assumed to be an infinite bus. The analysis does not lose generality since system equilibria require that $\omega_{n_G} = 0$.

$$\begin{aligned}
\dot{\mathbf{x}}_{dc} &= \mathbf{h}_{dc}(\mathbf{V}_{dc}, \mathbf{x}_{dc}, \mathbf{y}_{dc}) \\
\dot{\boldsymbol{\delta}}_G &= \boldsymbol{\omega}_G \\
\mathbf{M}_G\dot{\boldsymbol{\omega}}_G &= \mathbf{f}_G(\boldsymbol{\delta}, \mathbf{V}) - \mathbf{D}_G\boldsymbol{\omega}_G \\
\mathbf{D}_x\dot{\mathbf{V}}_G &= \mathbf{g}_G(\boldsymbol{\delta}, \mathbf{V}) \\
\mathbf{D}_L\dot{\boldsymbol{\delta}}_L &= \mathbf{f}_L(\boldsymbol{\delta}, \mathbf{V}, \lambda) \\
\mathbf{0} &= \begin{bmatrix} \mathbf{g}_L(\boldsymbol{\delta}, \mathbf{V}, \lambda) \\ \mathbf{f}_{dc}(\boldsymbol{\delta}, \mathbf{V}, \mathbf{x}_{dc}, \mathbf{y}_{dc}) \\ \mathbf{g}_{dc}(\boldsymbol{\delta}, \mathbf{V}, \mathbf{x}_{dc}, \mathbf{y}_{dc}) \end{bmatrix} \\
\mathbf{0} &= \mathbf{w}_{dc}(\mathbf{V}_{dc}, \mathbf{x}_{dc}, \mathbf{y}_{dc})
\end{aligned} \tag{7}$$

Matrices $\mathbf{M}_G$, $\mathbf{D}_G$, $\mathbf{D}_x$, and $\mathbf{D}_L$ are all positive definite diagonal constant matrices.

## BIFURCATIONS AND EIGENVALUES

It will prove convenient to define a composite vector that groups all state variables defined by the differential equations, and a second vector that groups all variables defined by the algebraic constraints. Let $\mathbf{z} = [\mathbf{x}_{dc}^T\ \boldsymbol{\delta}_G^T\ \boldsymbol{\omega}_G^T\ \mathbf{V}_G^T\ \boldsymbol{\delta}_L^T]^T$, and $\mathbf{u} = \left[[\mathbf{V}_L^T\ \boldsymbol{\delta}_{dc}^T\ \mathbf{V}_{dc}^T]\ \mathbf{y}_{dc}^T\right]^T$. Similarly, define a composite vector function, $\hat{\mathbf{f}}(\cdot)$, that groups all the terms representing the right hand side of differential equations, and a composite vector function, $\hat{\mathbf{g}}(\cdot)$, that groups all terms representing algebraic constraints. When the algebraic constraints $\hat{\mathbf{g}}(\cdot)$ have an invertible Jacobian $D_u\hat{\mathbf{g}}_\lambda$ along the system trajectories of interest, the algebraic variables can be eliminated (Implicit Function Theorem [10]), and (7) reduces to:

$$\left.\begin{aligned} \mathbf{M}\ \dot{\mathbf{z}} &= \hat{\mathbf{f}}_\lambda(\mathbf{z}, \mathbf{u}) \\ \mathbf{0} &= \hat{\mathbf{g}}_\lambda(\mathbf{z}, \mathbf{u}) \end{aligned}\right\} \quad \mathbf{M}\ \dot{\mathbf{z}} = \hat{\mathbf{f}}_\lambda(\mathbf{z}, \hat{\mathbf{h}}_\lambda(\mathbf{z})) = \mathbf{s}(\mathbf{z}, \lambda) \tag{8}$$

where $\mathbf{M}$ is a positive definite diagonal constant matrix.

A bifurcation [11, 12], or structural instability, occurs when the Jacobian $D_z\mathbf{s}(\cdot)$ of (8) is singular at the equilibrium $(\mathbf{z}_0, \lambda_0)$. Several types of bifurcation are possible in this situation, but of these only the saddle-node bifurcation occurs generically so that it is expected to be typical in practice [11, 13]. (More formally: a general one parameter family of differential equations such as (8) with singular Jacobian at an equilibrium can be perturbed to produce saddle-node bifurcations, and saddle-node bifurcations are robust to perturbations in the model.) The saddle-node is characterized by 2 equilibria coalescing and then disappearing as the parameter (e.g., load power) increases. Moreover the following conditions [11] generically apply at $(\mathbf{z}_0, \lambda_0)$:

1. $D_z\mathbf{s}(\mathbf{z}_0, \lambda_0)$ has a simple and unique zero eigenvalue, with right eigenvector $\mathbf{v}$ and left eigenvector $\mathbf{w}$, i.e., $D_z\mathbf{s}(\mathbf{z}_0, \lambda_0)\ \mathbf{v} = \mathbf{0}$ and $\mathbf{w}^T\ D_z\mathbf{s}(\mathbf{z}_0, \lambda_0) = \mathbf{0}$.
2. $$\mathbf{w}^T\ \left.\frac{\partial \mathbf{s}}{\partial \lambda}\right|_{(z_0, \lambda_0)} \neq 0. \tag{9}$$
3. $$\mathbf{w}^T\ \left[D_z^2\mathbf{s}(\mathbf{z}_0, \lambda_0)\ \mathbf{v}\right]\mathbf{v} \neq 0. \tag{10}$$

In equation (10) the square bracketed product of the 3-tensor $D_z^2\mathbf{s}\big|_0$ and the eigenvector $\mathbf{v}$ yields a matrix.

Conditions 1 through 3 guarantee generic quadratic behavior (i.e., two solutions joining into one) near the bifurcation point, and also prevent singularities of the composite Jacobian in the Newton-Raphson based method for finding saddle-nodes described below. Examples of such saddle-nodes occurring in ac/dc systems are illustrated in the sample system to follow.

An important computational issue in bifurcation studies for power systems is the relationship between eigenvalues of the power flow Jacobian $\mathbf{J}_{PF}$ and those

of the system dynamics linearized at the equilibrium point, denoted by $\mathbf{J}_{TS} = \mathbf{M}^{-1} D_z \mathbf{s}(\mathbf{z}_0, \lambda_0)$. This subject has been examined for simpler system models in [14, 15, 16]. The following discussion demonstrates that singularity (zero eigenvalue) of the power flow Jacobian implies a zero eigenvalue for the linearized system dynamics. Linearizing $\hat{\mathbf{f}}(\cdot)$ and $\hat{\mathbf{g}}(\cdot)$ at the equilibrium yields a block Jacobian of the form:

$$D(\hat{\mathbf{f}}, \hat{\mathbf{g}})|_0 = \left[\begin{array}{c|c} D_z \hat{\mathbf{f}}_\lambda|_0 & D_u \hat{\mathbf{f}}_\lambda|_0 \\ \hline D_z \hat{\mathbf{g}}_\lambda|_0 & D_u \hat{\mathbf{g}}_\lambda|_0 \end{array}\right]$$

Eliminating the algebraic variables yields the Jacobian for the reduced dynamic system, i.e.,

$$\mathbf{M}\,\mathbf{J}_{TS} = D_z \hat{\mathbf{f}}_\lambda|_0 - D_u \hat{\mathbf{f}}_\lambda|_0 D_u \hat{\mathbf{g}}_\lambda|_0{}^{-1} D_z \hat{\mathbf{g}}_\lambda|_0$$

which can be shown to have the following structure:

$$\mathbf{M}\,\mathbf{J}_{TS} = \begin{array}{c} \\ \dot{\mathbf{x}}_{dc} \\ \dot{\boldsymbol{\delta}}_G \\ \mathrm{M}_G \dot{\boldsymbol{\omega}}_G \\ \mathrm{D}_x \dot{\mathrm{V}}_G \\ \mathrm{D}_L \dot{\boldsymbol{\delta}}_L \end{array} \begin{array}{c} \begin{array}{ccccc} \mathbf{x}_{dc} & \boldsymbol{\delta}_G & \boldsymbol{\omega}_G & \mathrm{V}_G & \boldsymbol{\delta}_L \end{array} \\ \left[\begin{array}{ccccc} \mathbf{P}_1 & \mathbf{P}_2 & \mathbf{0} & \mathbf{P}_3 & \mathbf{P}_4 \\ \mathbf{0} & \mathbf{0} & \mathbf{I}_{n_G-1} & \mathbf{0} & \mathbf{0} \\ \mathbf{P}_5 & \mathbf{P}_6 & -\mathbf{D}_G & \mathbf{P}_7 & \mathbf{P}_8 \\ \mathbf{P}_9 & \mathbf{P}_{10} & \mathbf{0} & \mathbf{P}_{11} & \mathbf{P}_{12} \\ \mathbf{P}_{13} & \mathbf{P}_{14} & \mathbf{0} & \mathbf{P}_{15} & \mathbf{P}_{16} \end{array}\right] \end{array}$$

Then, using standard block determinant formulas, the determinant of $\mathbf{J}_{TS}$ can be calculated:

$$\begin{aligned} \mathrm{det}\mathbf{J}_{TS} &= (-1)^k\, \mathrm{det}\mathbf{M}^{-1}\, \mathrm{det} \begin{vmatrix} \mathbf{P}_1 & \mathbf{P}_2 & \mathbf{P}_3 & \mathbf{P}_4 \\ \mathbf{P}_5 & \mathbf{P}_6 & \mathbf{P}_7 & \mathbf{P}_8 \\ \mathbf{P}_9 & \mathbf{P}_{10} & \mathbf{P}_{11} & \mathbf{P}_{12} \\ \mathbf{P}_{13} & \mathbf{P}_{14} & \mathbf{P}_{15} & \mathbf{P}_{16} \end{vmatrix} \\ &= (-1)^k\, \frac{\mathrm{det}\mathbf{P}}{\mathrm{det}\mathbf{M}} \end{aligned} \tag{11}$$

where $k$ is a positive integer.

On the other hand, the power flow Jacobian can be obtained from (7) with $\boldsymbol{\omega}_G = 0$, and it can be shown that:

$$\mathrm{det}\mathbf{J}_{PF} = \mathrm{det}\mathbf{P}\ \mathrm{det} D_u \hat{\mathbf{g}}_\lambda|_0 \tag{12}$$

Hence, from (11) and (12):

$$\mathrm{det}\mathbf{J}_{TS} = (-1)^k \frac{\mathrm{det}\mathbf{J}_{PF}}{\mathrm{det}\mathbf{M}\ \mathrm{det} D_u \hat{\mathbf{g}}_\lambda|_0} \tag{13}$$

Thus, it suffices to look for zero eigenvalues of $\mathbf{J}_{PF}$ in order to identify singularities of the full linearized dynamics.

## THE POINT OF COLLAPSE METHOD

This technique augments the equations for equilibria with constraints ensuring a zero eigenvalue at the point of interest. This approach is described by Seydel [12], and was applied to voltage stability analysis of ac systems in [17]. The equations for $\mathbf{z}$, $\mathbf{v}$, and $\lambda$ take the following form:

$$\begin{aligned} \mathbf{s}(\mathbf{z}, \lambda) &= \mathbf{0} \\ D_z \mathbf{s}(\mathbf{z}, \lambda)\ \mathbf{v} &= \mathbf{0} \\ \mathbf{v} &\neq \mathbf{0} \end{aligned} \tag{14}$$

Solving (14) is equivalent to solving equations (15) below for $\tilde{\mathbf{z}} = [\mathbf{x}_{dc}^T\ \boldsymbol{\delta}_G^T\ \mathbf{V}_G^T\ \boldsymbol{\delta}_L^T]^T$, $\mathbf{u}$, $\hat{\mathbf{v}}$, and $\lambda$, since under the assumption of $D_u \hat{\mathbf{g}}_\lambda|_0$ invertible, singularity of the "power flow" Jacobian is necessary and sufficient for singularity of $D_z \mathbf{s}$.

$$\begin{aligned} \begin{bmatrix} \tilde{\mathbf{f}}_\lambda(\tilde{\mathbf{z}}, \mathbf{u}) \\ \hat{\mathbf{g}}_\lambda(\tilde{\mathbf{z}}, \mathbf{u}) \end{bmatrix} &= \mathbf{0} \\ \begin{bmatrix} D_{\tilde{z}} \tilde{\mathbf{f}}_\lambda & D_u \tilde{\mathbf{f}}_\lambda \\ D_{\tilde{z}} \hat{\mathbf{g}}_\lambda & D_u \hat{\mathbf{g}}_\lambda \end{bmatrix} \begin{bmatrix} \hat{\mathbf{v}}_{\tilde{z}} \\ \hat{\mathbf{v}}_u \end{bmatrix} &= \mathbf{0} \\ \begin{bmatrix} \hat{\mathbf{v}}_{\tilde{z}} \\ \hat{\mathbf{v}}_u \end{bmatrix} &\neq \mathbf{0} \end{aligned} \tag{15}$$

Here we have that $\tilde{\mathbf{f}}_\lambda(\cdot) = [\mathbf{h}_{dc}^T(\cdot)\ \mathbf{f}_G^T(\cdot)\ \mathbf{g}_G^T(\cdot)\ \mathbf{f}_L^T(\cdot)]^T$.

From the matrix structure of $\mathbf{J}_{TS}$ and $\mathbf{J}_{PF}$, it can be shown that the right eigenvectors $\mathbf{v}$ in (14) and $\hat{\mathbf{v}}_{\tilde{z}}$ in (15) are the same up to a zero component, i.e.,

$$\hat{\mathbf{v}}_{\tilde{z}} = \begin{bmatrix} \hat{\mathbf{v}}_{x_{dc}} \\ \hat{\mathbf{v}}_{\delta_G} \\ \hat{\mathbf{v}}_{V_G} \\ \hat{\mathbf{v}}_{\delta_L} \end{bmatrix} \Rightarrow\ \mathbf{v} = \begin{bmatrix} \mathbf{v}_{x_{dc}} \\ \mathbf{v}_{\delta_G} \\ \mathbf{v}_{\omega_G} \\ \mathbf{v}_{V_G} \\ \mathbf{v}_{\delta_L} \end{bmatrix} = \begin{bmatrix} \hat{\mathbf{v}}_{x_{dc}} \\ \hat{\mathbf{v}}_{\delta_G} \\ \mathbf{0} \\ \hat{\mathbf{v}}_{V_G} \\ \hat{\mathbf{v}}_{\delta_L} \end{bmatrix}$$

The nonzero condition for the eigenvector can be guaranteed by requiring a particular component of $\hat{\mathbf{v}}_{\tilde{z}}$ to be equal to one ($\hat{v}_i = 1$). (Replacing $\mathbf{v} \neq \mathbf{0}$ by $\hat{v}_i = 1$ fails in the unlikely event of equations (15) yielding a nonzero eigenvector such that $\hat{v}_i = 0$.)

This technique also yields the eigenvector at the bifurcation point, offering insight into the local dynamic

behavior of the system close to bifurcation, as described in [13].

An alternative method for finding the bifurcation point is to impose conditions 1 and 2 of a saddle-node to the composite function $\left[\tilde{\mathbf{f}}_\lambda^T(\tilde{\mathbf{z}},\mathbf{u})\ \hat{\mathbf{g}}_\lambda^T(\tilde{\mathbf{z}},\mathbf{u})\right]^T$. This is equivalent to the approach proposed by Van Cutsem for an ac system in [18], where a Lagrangian of the reactive power flow is used to find the bifurcation. Equation (16) below defines the constraints used in this approach. Note that equations (16) are essentially the same as (15) except that the *left* zero eigenvector $\hat{\mathbf{w}}$ is used to ensure singularity.

$$\begin{bmatrix} \tilde{\mathbf{f}}_\lambda(\tilde{\mathbf{z}},\mathbf{u}) \\ \hat{\mathbf{g}}_\lambda(\tilde{\mathbf{z}},\mathbf{u}) \end{bmatrix} = \mathbf{0} \quad (16a)$$

$$\begin{bmatrix} \hat{\mathbf{w}}_{\tilde{z}}^T & \hat{\mathbf{w}}_u^T \end{bmatrix} \begin{bmatrix} D_{\tilde{z}}\tilde{\mathbf{f}}_\lambda & D_u\tilde{\mathbf{f}}_\lambda \\ D_{\tilde{z}}\hat{\mathbf{g}}_\lambda & D_u\hat{\mathbf{g}}_\lambda \end{bmatrix} = \mathbf{0} \quad (16b)$$

$$\begin{bmatrix} \hat{\mathbf{w}}_{\tilde{z}}^T & \hat{\mathbf{w}}_u^T \end{bmatrix} \begin{bmatrix} \partial\tilde{\mathbf{f}}_\lambda/\partial\lambda \\ \partial\hat{\mathbf{g}}_\lambda/\partial\lambda \end{bmatrix} = K \quad (16c)$$

$K$ is an arbitrary nonzero scalar (such as $K=-1$), and

$$\frac{\partial\tilde{f}_{\lambda_i}}{\partial\lambda} = \begin{cases} \Delta P_l & \text{if } \tilde{f}_{\lambda_i} = f_{L_l} \\ 0 & \text{otherwise} \end{cases}$$

$$\frac{\partial\hat{g}_{\lambda_i}}{\partial\lambda} = \begin{cases} \Delta Q_l & \text{if } \hat{g}_{\lambda_i} = g_{L_l} \\ 0 & \text{otherwise} \end{cases}$$

Equation (16c) is equivalent to (9) for the reduced system differential equations (8), assuming $D_u\hat{\mathbf{g}}_{\lambda_0}(\tilde{\mathbf{z}}_0,\mathbf{u}_0)$ is nonsingular and exploiting the matrix structure of $\mathbf{J}_{TS}$ and $\mathbf{J}_{PF}$. See the Appendix for a formal proof of this statement.

The constraint equations defined above may have several solutions, indicating that the system model could have different parameter values yielding several bifurcation points. However, since a Newton-Raphson method is employed for finding the bifurcations, a good starting guess for the eigenvectors typically puts the initial condition within the region of attraction of the desired solution. A technique to obtain this initial guess and the computational issues involved in applying the Point of Collapse method are discussed later.

Because the system model represents limits (and hence has discontinuous derivatives), it is necessary to check whether a controller limit has been exceeded at the bifurcation point solution. HVDC converter transformer tap changers can also be included in the analysis, although several studies carried out by the authors have shown that these elements do not have a significant effect in the bifurcation point due to its limited voltage control range (see example in the next section). Nevertheless, the equation structure can be changed in these cases to reflect switches in current controllers and transformer taps, so that further analyses of the stability of the new equilibrium can be carried out.

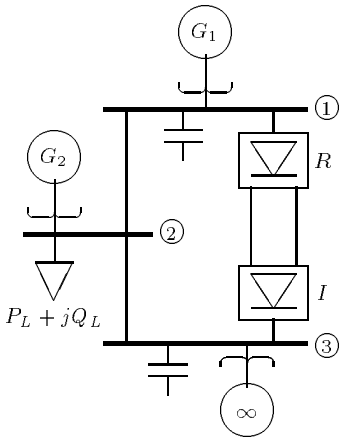


**Fig. 3**: *Sample ac/dc system*

## VOLTAGE PROFILES AT BIFURCATION FOR A SAMPLE SYSTEM

Figure 3 depicts the reduced ac/dc system examined in this section. This system is a steady-state equivalent at the three buses of interest of the interconnected power systems in the western part of the United States. Generator $G_2$ supports the voltage at the intermediate load bus, and bus 1 has relatively strong voltage support from generator $G_1$. The effective short circuit ratio (ESCR) at bus 1 is 6.2, while the ESCR at the inverter side is 4.0. The dc line is designed to supply about two thirds of the power needed at bus 3, and the initial load at bus 2 is $P_L^0 = 475$ MW and $Q_L^0 = 156.1$ MVAR. Tables 1 and 2 depict all the ac/dc test system data, with generators simulated as constant voltage sources.

For variations in the load at bus 2, a computer assisted symbolic algebra package [19, 20] was used to obtain profiles for the three bus voltage magnitudes shown in Figs. 4 through 7. Figures 4 and 5 show the "nose" curves (bifurcation diagrams) for changes in the power demand at bus 2, when VDCOLs are not considered. Full dynamic analysis shows that the equilibria with voltage magnitudes higher than those at the point of collapse (saddle-node bifurcation) are stable, whereas equilibria with voltages below this point are unstable. Figure 4 shows three additional bifurcation points in the unstable region, and also sharp turning points due to changes in the control modes of the HVDC link. This behavior is different from the behavior of an ac only system (at least for the type of ac model employed here), since in such systems the expected shape of the "nose" curves is approximately globally quadratic as shown in [21] (similar to the profiles depicted in Figs. 5 and 7). The unique character of the combined ac and HVDC system is more evident when VDCOLs are included as shown in Figs. 6 and 7. Here the ac/dc system has a completely different set of unstable equilibria, suggesting that significant changes in the stability region of the ac/dc system have taken place; also, the points of col-

| Element | $G$ | $B$ | $-B_s$ |
|---|---|---|---|
| Line 1–2 | 3.68 | 54.13 | 4.68 |
| Line 2–3 | 3.68 | 54.13 | 4.68 |
| Transf. $G_1$ | | 166.67 | |
| Transf. $G_2$ | | 100.00 | |
| Transf. $\infty$ | | 100.00 | |
| Capac. 1 | | | 13.00 |
| Capac. 3 | | | 13.68 |

**Table 1**: *AC transmission system data. All quantities are in p.u. for a 550 kV and 100 MVA base.*

| Variable | Rectifier | Inverter |
|---|---|---|
| $a$ | 1.7634 | 1.7678 |
| $X_c$ | 0.1345 | 0.1257 |
| $\alpha_{min}$ | $5^0$ | $\sim 120^{0\dagger}$ |
| $\alpha_{max}$ | $120^0$ | $\sim 142^{0\dagger}$ |
| $\gamma_{min}$ | $\sim 40^{0\dagger}$ | $18^0$ |
| $\gamma_{max}$ | $\sim 155^{0\dagger}$ | $40^0$ |
| $I_o$ | 1.0 | 0.9 |
| $I_{o_{min}}{}^{\ddagger}$ | 0.1 | 0.0 |
| $V_{ac_{max}}{}^{\ddagger}$ | 0.95 | 0.95 |
| $V_{ac_{min}}{}^{\ddagger}$ | 0.5 | 0.5 |
| $R_d$ | 0.0624 | — |

$^{\dagger}$Assuming $\mu \approx 20^0$ $^{\ddagger}$VDCOL

**Table 2**: *DC system data. All quantities are in p.u. for a 550 kV and 2.5 kA base.*

lapse have changed, i.e., the loadability margin of the system is altered by the inclusion of VDCOLs.

All these figures, especially 4 and 6, show that the stable equilibrium region of bus voltage $V_1$ remains approximately constant throughout the system loading, due to the relatively strong voltage support from generator $G_1$ and the HVDC filtering system. Hence, the VSF ($\mathrm{d}V/\mathrm{d}Q$) criteria is not a good measure of proximity to voltage collapse in this case since its value remains almost unchanged during most of the study.

Table 3 shows the values of system variables at the point of collapse, obtained by solving equations (15) for active and reactive power at the system load. For the case where VDCOLs are not included, the voltage magnitudes at bifurcation are higher when collapse is reached via active load increase as compared to reactive increase, which is reasonable due to the high reactive demands in the latter case. Although the points of collapse do not change significantly when VDCOLs are included, finding the unstable equilibrium point becomes more difficult since the controller current order changes with the ac voltage. Nevertheless, finding the bifurcation points with the PoC method is straight forward. This makes the method very appealing when compared to other methods that need to calculate the unstable equilibrium points (e.g., [8]), since the degree of difficulty has not changed in the PoC method with the mode of operation of the HVDC system.

Based on the bifurcation values for active power load, the system has a large "maximum loadability" due in part to the infinite bus and the transmission line design. The active load changes are supplied mainly by the infinite bus, whereas the reactive increase is supported by the generators at buses 1 and 2; this in part explains the smaller reactive bifurcation values. Note that although the loadability margin changes when VDCOLs are included, one cannot draw a definite conclusion regarding the advantages or disadvantages of this mode of operation from the point of view of saddle-node bifurcations.

| Var. | $\Delta P_L$ No VDCOL | $\Delta Q_L$ No VDCOL | $\Delta P_L$ VDCOL | $\Delta Q_L$ VDCOL |
|---|---|---|---|---|
| $\lambda$ | 44.66 | 21.96 | 46.84 | 20.05 |
| $\delta_1$ | $-43.6^0$ | $84.7^0$ | $-44.5^0$ | $84.2^0$ |
| $\delta_2$ | $-66.1^0$ | $58.7^0$ | $-75.0^0$ | $58.7^0$ |
| $\delta_3$ | $-6.0^0$ | $29.1^0$ | $-8.1^0$ | $29.1^0$ |
| $\delta_{g_1}$ | $-28.2^0$ | $100.^0$ | $-28.9^0$ | $99.7^0$ |
| $\delta_{g_2}$ | $-62.8^0$ | $62.3^0$ | $-71.4^0$ | $61.1^0$ |
| $V_1$ | 0.904 | 0.882 | 0.889 | 0.902 |
| $V_2$ | 0.812 | 0.749 | 0.766 | 0.778 |
| $V_3$ | 0.802 | 0.782 | 0.773 | 0.812 |
| $I_d$ | 1.000 | 1.000 | 0.878 | 0.904 |
| $V_{d_r}$ | 1.763 | 1.717 | 1.705 | 1.792 |
| $V_{d_i}$ | 1.701 | 1.655 | 1.650 | 1.735 |
| $\alpha_r$ | $28.5^0$ | $28.5^0$ | $30.9^0$ | $27.4^0$ |
| $\gamma_i$ | $18.0^0$ | $18.0^0$ | $18.0^0$ | $18.0^0$ |

**Table 3**: *Points of collapse for $V_{g_1} = V_{g_2} = V_{g_3} = 1$. Voltages and currents are in p.u., with $V_n = 550$ kV, $I_n = 2.5$ kA, and $S_n = 100$ MVA.*

High level control modes for the HVDC system (e.g., power modulation) and transformer tap changers can easily be included in the PoC method. The idea is to find the initial bifurcation point without enforcing limits, check whether any limits have been violated, and then reapply the method to find the new saddle-node. The effect of taps in the converter transformers was simulated assuming a $\pm 10\%$ regulating range for the system in Fig. 3, obtaining a 1% variation in the bifurcation point.

Another interesting characteristic of the sample ac/dc system relates to the behavior of the eigenvalues before bifurcation. As shown in Fig. 8, a complex conjugate pair crosses the imaginary axis as the system load increases (at 4682 MW of additional load), this happens even before the system becomes unstable due to voltage collapse. This phenomenon is known as Hopf bifurcation and is described with more detail in a later section.

## COMPUTATIONAL ISSUES

One of the main concerns when applying the Point of Collapse method is the singularity of the power flow Jacobian at the bifurcation point, which might lead one to believe that equations (16) or (15) are ill-conditioned with respect to a Newton-Raphson solution algorithm. Let $\mathbf{F}(\cdot) = [\tilde{\mathbf{f}}^T(\cdot)\ \hat{\mathbf{g}}^T(\cdot)]^T$ and $\mathbf{y} = [\tilde{\mathbf{z}}^T\ \mathbf{u}^T]^T$, then equations (16) become:

$$D_y \mathbf{F}^T(\mathbf{y}, \lambda)\hat{\mathbf{w}}_y = \mathbf{0} \qquad (17)$$

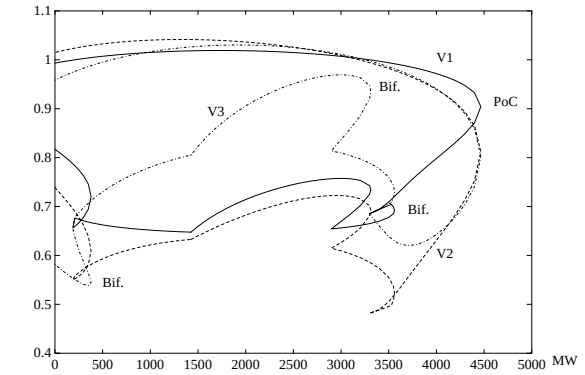


**Fig. 4**: *AC voltage profiles for active power changes at load bus 2 ($\Delta P_2 = 1$, $\Delta Q_2 = 0$). No VDCOL.*

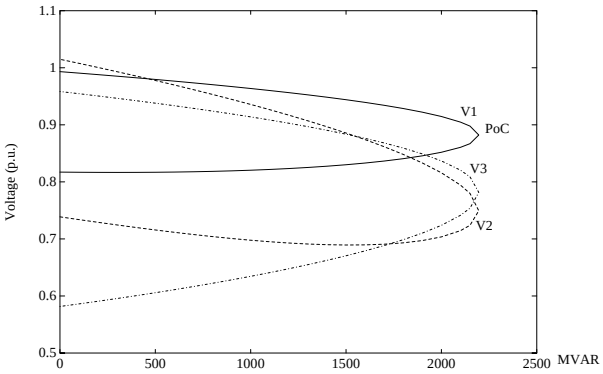


**Fig. 5**: *AC voltage profiles for reactive power changes at load bus 2 ($\Delta P_2 = 0$, $\Delta Q_2 = 1$). No VDCOL.*

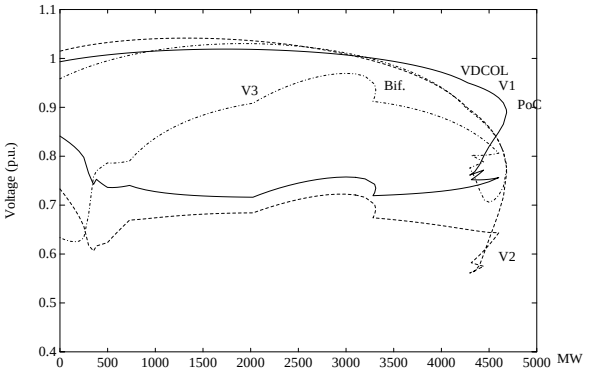


**Fig. 6**: *AC voltage profiles for active power changes at load bus 2 ($\Delta P_2 = 1$, $\Delta Q_2 = 0$). VDCOL included.*

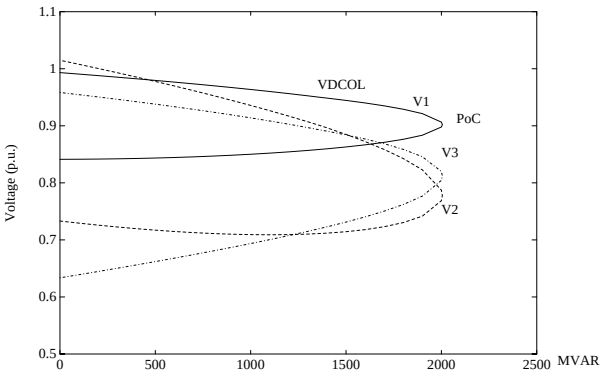


**Fig. 7**: *AC voltage profiles for reactive power changes at load bus 2 ($\Delta P_2 = 0$, $\Delta Q_2 = 1$). VDCOL included.*

$$\begin{aligned} \mathbf{F}(\mathbf{y}, \lambda) &= \mathbf{0} \\ \frac{\partial \mathbf{F}}{\partial \lambda}^T \hat{\mathbf{w}}_y &= K \end{aligned}$$

Now, since $\mathbf{F}(\mathbf{y}, \lambda)$ is linear with respect to $\lambda$, the Jacobian $\mathbf{J}_{PoC}$ of equations (17) is:

$$\mathbf{J}_{PoC} = \begin{bmatrix} D_y^2 \mathbf{F}^T \hat{\mathbf{w}}_y & D_y \mathbf{F}^T & \mathbf{0} \\ D_y \mathbf{F} & \mathbf{0} & \frac{\partial \mathbf{F}}{\partial \lambda} \\ \mathbf{0} & \frac{\partial \mathbf{F}}{\partial \lambda}^T & 0 \end{bmatrix} \qquad (18)$$

Although the individual block $D_y \mathbf{F}(\mathbf{y}_0, \lambda_0)$ is singular, conditions (9) and (10) imply that $\mathbf{J}_{PoC}$ is nonsingular [22].

The Jacobian $\mathbf{J}_{PoC}$ is symmetric for an ac lossless system [18], and topology-symmetric for a general ac system. However, the equations for the HVDC links cause the power flow Jacobian to be rather unsymmetric. Furthermore, for an ac system this Jacobian has an special structure that can be exploited using blocking techniques to reduce the computational burden [18], but once the dc system is included in the analysis this structure is partially lost. Nevertheless, one can still use matrix blocking techniques to improve the computational characteristics of the proposed method.

An important issue in solving the Point of Collapse equations by Newton's method is the choice of initial guess for eigenvectors $\hat{\mathbf{v}}_y$ or $\hat{\mathbf{w}}_y$. The approach used here is to apply several iterations of the Inverse Power Method [23] to the power flow Jacobian. This typically yields a vector close to the span of the real and imaginary parts of the eigenvector(s) corresponding to the eigenvalue(s) with the smallest magnitude. Although this is not absolutely guaranteed to be the eigenvalue that eventually goes to zero at bifurcation, it is quite likely. The method has proven effective in a number of sample ac and ac/dc systems, and often produces a good initial guess in just one iteration.

With a proper initial guess, the computational costs of solving (15), or (16) are somewhat higher than those for the original power flow equations. The number of equations has doubled, but the Jacobian $\mathbf{J}_{PoC}$ retains its sparsity. Furthermore, close to the bifurcation point the power flow Jacobian $\mathbf{J}_{PF}$ becomes ill-conditioned, causing slow convergence for power flow methods and continuation methods [21], whereas the Jacobian for the proposed Newton solution is far from singularity.

Research currently under way on computation of points of collapse using the proposed technique in systems with over 100 buses, suggests solution times in the order of 10 to 20 ordinary power flows. However, more work has to be done on this area before reaching definite conclusions.

## HOPF BIFURCATIONS

Hopf bifurcation is another mechanism of transition to instability in dynamical systems. This phenomenon

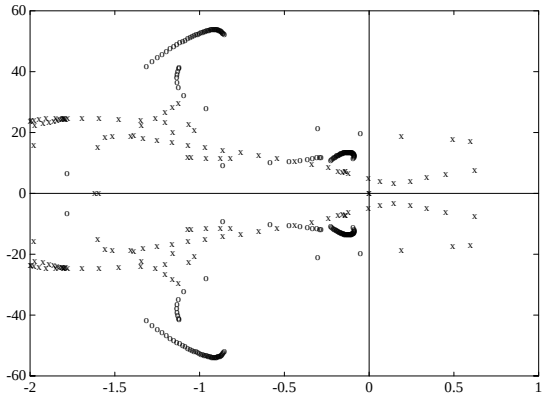


**Fig. 8**: *Eigenvalues for the stable (o) and unstable (x) equilibria for active power changes at bus 2. VDCOL included.*

is characterized by complex eigenvalues of the linearized system dynamics crossing the imaginary axis as the system parameters change [11, 12]. This type of bifurcation has been proven not to exist for simple ac lossless system models [24]. However, it has been observed in more detailed ac system models that consider transfer conductances and exciter dynamics [25].

These bifurcations were observed for the ac/dc system examined here, as shown in the eigenvalue-locus of Fig. 8 obtained when the active power at bus 2 is increased and VDCOLs are included. Here complex conjugate eigenvalues of a stable equilibrium crosses the imaginary axis from left to right, slightly before the system reaches a saddle-node. This makes the system unstable by a different mechanism than voltage collapse. The interested reader is referred to [26] for a description of computational techniques for finding these bifurcations in nonlinear power system models.

## CONCLUSIONS

A thorough analysis of bifurcation phenomena in a particular model of ac/dc systems is presented. The Point of Collapse method is shown to be computational feasible as a means to determine acceptable load increase before encountering voltage collapse in ac/dc systems. Moreover, it appears particularly promising when HVDC lines with controller limits and VDCOLs are considered.

The results presented here justify further studies in larger systems of the proposed method. The authors are currently working in implementing the PoC method for arbitrary ac/dc system dimensions in a UNIX workstation environment using C code.

## ACKNOWLEDGEMENTS

The support of this work by the Electric Power Research Institute project RP 2675-4 and National Science Foundation grants ECS-8857019, ECS-9009079, and ECS-8907391 is gratefully acknowledged. Also the authors would like to thank Stig Nilsson of EPRI for his valuable comments and suggestions.

## REFERENCES

[1] *Proceedings: Bulk Power System Voltage Phenomena—Voltage Stability and Security*, EPRI EL-6183, Jan. 1989.

[2] *Methodology of Integration of HVDC Links in Large AC Systems—Phase 1: Reference Manual*, EPRI EL-3004, March 1983.

[3] *Methodology of Integration of HVDC Links in Large AC Systems—Phase 2: Advanced Concepts*, EPRI EL-4365, Vol. 1, April 1987.

[4] J. Arrillaga, *High Voltage Direct Current Transmission*, Peter Peregrinus Ltd., London, UK, 1983.

[5] J. Arrillaga, C. P. Arnold, B. J. Harker, *Computer Modelling of Electrical Power Systems*, John Wiley & Sons, UK, 1983.

[6] A. E. Hammad and W. Kuhn, "A Computation Algorithm for Assessing Voltage Stability at AC/DC Interconnections," *IEEE Trans. Power Systems*, Vol.1, No. 1, Feb. 1986, pp. 209–216.

[7] B. Frankén and G. Andersson, "Analysis of HVDC converters connected to Weak AC Systems," *IEEE Trans. Power Systems*, Vol. 5, No. 1, Feb. 1990, pp. 235–242.

[8] Y. Tamura, K. Sakamoto and Y. Tayama, "Current Issues in the Analysis of Voltage Instability Phenomena," pp. 5.39–5.53 in [1].

[9] C. L. DeMarco, T. J. Overbye, "An Energy Based Security Measure for Assessing Vulnerability to Voltage Collapse," *IEEE Trans. Power Systems*, Vol.5, No. 2, May 1990, pp. 419–427..

[10] W. Rudin, *Principles of Mathematical Analysis*, Third Edition, McGraw-Hill, USA, 1976.

[11] J. Guckenheimer and P. Holmes, *Nonlinear Oscillations, Dynamical Systems, and Bifurcations of Vector Fields*, Springer-Verlag, New York, USA, 1986.

[12] R. Seydel, *From Equilibrium to Chaos—Practical Bifurcation and Stability Analysis*, Esevier Science Publishers, North-Holland, 1988.

[13] I. Dobson and H. D. Chiang, "Towards a Theory of Voltage Collapse in Electric Power Systems," *Systems & Control Letters 13*, 1989, pp. 253–262.

[14] H. G. Kwatny, "Steady State Analysis of Voltage Instability Phenomena," pp. 5.1–5.22 in [1].

[15] S. Sastry and P. P. Variaya, "Hierarchical Stability and Alert State Steering Control of Interconnected Power Systems," *IEEE Trans. Circuits and Systems*, Vol. 27, No. 11, Nov. 1980, pp. 1102–1112.

[16] P. W. Sauer and M. A. Pai, "Power System Steady-State Stability and the Load Flow Jacobian," *IEEE/PES 89 SM 682-6 PWRS*, July 1989.

[17] F. L. Alvarado and T. H. Jung, "Direct Detection of Voltage Collapse Conditions," pp. 5.23–5.38 in [1].

[18] T. Van Cutsem, "A Method to Compute Reactive Power Margins with respect to Voltage Collapse," *IEEE/PES 90 WM 097-6 PWRS*, Feb. 1990.

[19] F. L. Alvarado, *Solver-Q Instruction Manual*, Software Development Distribution Center, University of Wisconsin-Madison, 1987.

[20] F. L. Alvarado and D. J. Ray, "Symbolically-assisted Numeric Computation in Education," *Int. J. Appl. Engr. Ed.*, Vol. 4, No. 6, pp. 519–536, 1988.

[21] K. Iba, H. Suzuki, M. Egawa and T. Watanabe, "Calculation of Critical Loading Condition with Nose Curve Using Homotopy Continuation Method," *IEEE/PES 90 SM 415-0 PWRS*, July 1990.

[22] A. Spence and B. Werner, "Non-simple Turning Points and Cusps," *IMA J. Num. Analysis* **2**, 1982, pp. 413-427.

[23] S. D. Conte and Carl de Boor, *Elementary Numerical Analysis—An Algorithmic Approach*, Third Edition, McGraw-Hill, New York, USA, 1980.

[24] H. D. Chiang and F. F. Wu, "Stability of Nonlinear Systems Described by a Second-Order Vector Differential Equation," *IEEE Trans. Circuits and Systems*, Vol. 35, No. 6, June 1988, pp 703–711.

[25] E. H. Abed and P. P. Varaiya, "Nonlinear Oscillations in Power Systems," *International Journal of Electric Power & Energy Systems*, Vol. 6, 1984, pp. 37–43.

[26] F. L. Alvarado, "Bifurcations in Nonlinear Systems: Computational Issues," *Proceedings of ISCAS*, New Orleans, Lousiana, May 1–3, 1990, pp. 922–925.

## APPENDIX: EQUIVALENCE OF SADDLE-NODE CONDITIONS

This appendix shows that (9) is equivalent to equation (16c). Let $D_u\hat{\mathbf{g}}(\cdot)$ be nonsingular at the equilibrium point $(\mathbf{z}_0, \mathbf{u}_0, \lambda_0)$ for equations (8). There exists a local function $\mathbf{h}(\cdot)$ around the equilibrium such that $\mathbf{u} = \mathbf{h}(\mathbf{z}, \lambda)$. Then,

$$\begin{aligned} \hat{\mathbf{g}}(\mathbf{z}, \mathbf{u}, \lambda) &= \hat{\mathbf{g}}(\mathbf{z}, \mathbf{h}(\mathbf{z}, \lambda), \lambda) = \mathbf{0} \\ \Rightarrow \left.\frac{\partial \mathbf{u}}{\partial \lambda}\right|_0 &= -D_u \hat{\mathbf{g}}|_0^{-1} \left.\frac{\partial \hat{\mathbf{g}}}{\partial \lambda}\right|_0 \end{aligned}$$

On the other hand, since $\mathbf{s}(\mathbf{z}, \mathbf{u}, \lambda) = \hat{\mathbf{f}}(\mathbf{z}, \mathbf{h}(\mathbf{z}, \lambda), \lambda)$:

$$\begin{aligned} \left.\frac{\partial \mathbf{s}}{\partial \lambda}\right|_0 &= \left.\frac{\partial \hat{\mathbf{f}}}{\partial \lambda}\right|_0 + D_u \hat{\mathbf{f}}|_0 \left.\frac{\partial \mathbf{u}}{\partial \lambda}\right|_0 \\ &= \left.\frac{\partial \hat{\mathbf{f}}}{\partial \lambda}\right|_0 - D_u \hat{\mathbf{f}}|_0 D_u \hat{\mathbf{g}}|_0^{-1} \left.\frac{\partial \hat{\mathbf{g}}}{\partial \lambda}\right|_0 \qquad \text{(A.1)} \end{aligned}$$

Now, from the ac/dc reduced differential equations (8) and condition 1 of a saddle-node it follows that

$$\hat{\mathbf{w}}_u^T = -\hat{\mathbf{w}}_z^T D_u \hat{\mathbf{f}}|_0 D_u \hat{\mathbf{g}}|_0^{-1} \qquad \text{(A.2)}$$

$$\mathbf{0} = \hat{\mathbf{w}}_z^T \underbrace{\left( D_z \hat{\mathbf{f}}|_0 - D_u \hat{\mathbf{f}}|_0 D_u \hat{\mathbf{g}}|_0^{-1} D_z \hat{\mathbf{g}}|_0 \right)}_{D_z \mathbf{s}|_0}$$

$$\Rightarrow \mathbf{w} = \hat{\mathbf{w}}_z \qquad \text{(A.3)}$$

Thus, from equations (A.1), (A.2), and (A.3) it can be seen that equations (9) and (16c) are equivalent, i.e.,

$$\begin{aligned} \mathbf{w}^T \left.\frac{\partial \mathbf{s}}{\partial \lambda}\right|_0 &= \hat{\mathbf{w}}_z^T \left.\frac{\partial \hat{\mathbf{f}}}{\partial \lambda}\right|_0 + \hat{\mathbf{w}}_u^T \left.\frac{\partial \hat{\mathbf{g}}}{\partial \lambda}\right|_0 \\ &= \hat{\mathbf{w}}_z^T \left.\frac{\partial \tilde{\mathbf{f}}}{\partial \lambda}\right|_0 + \hat{\mathbf{w}}_u^T \left.\frac{\partial \hat{\mathbf{g}}}{\partial \lambda}\right|_0 \\ &= \hat{\mathbf{w}}_y^T \frac{\partial \mathbf{F}}{\partial \lambda} = K \neq 0 \qquad \text{(A.4)} \end{aligned}$$

Similar arguments can be used to prove the equivalence of equation (10) and the corresponding saddle-node condition for the power flow equations, i.e.,

$$\mathbf{w}^T \left[ D_z^2 \mathbf{s}|_0 \mathbf{v} \right] \mathbf{v} = \hat{\mathbf{w}}_y^T \left[ D_y^2 \mathbf{F}\, \hat{\mathbf{v}}_y \right] \hat{\mathbf{v}}_y \neq 0 \qquad \text{(A.5)}$$

Based on (A.4) and (A.5), one can readily prove that the Point of Collapse Jacobian is nonsingular.

**Claudio A. Cañizares** (S'87) was born in Mexico, D.F. in 1960. In April 1984, he received the Electrical Engineer degree from the Escuela Politécnica Nacional (EPN), Quito-Ecuador, where he is currently an Assistant Professor on leave of absence, and the MSEE from the University of Wisconsin-Madison in 1988. Mr. Cañizares is a PhD student, T.A., and R.A. at the University of Wisconsin-Madison, sponsored by Fulbright, OAS, and EPN.

**Fernando L. Alvarado** (M'69, SM'78) was born in Lima, Peru. He received the BEE and PE degrees from the National University of Engineering in Lima, Peru, the MS degree from Clarkson University, and the PhD degree from the University of Michigan in 1972. Since 1975 he has been with the University of Wisconsin in Madison, where he is a Professor of Electrical and Computer Engineering.

**Christopher L. DeMarco** (S'80, M'85) was born in Derby, Connecticut in 1958. He received his Bachelor of Science degree in Electrical Engineering from the Massachusetts Institute of Technology in June of 1980, and his PhD degree in Electrical Engineering and Computer Sciences from the University of California, Berkeley in May 1985. In January 1985, he joined the faculty of the Department of Electrical and Computer Engineering at the University of Wisconsin-Madison.

**Ian Dobson** (M'89) received the BA in Mathematics from Cambridge, England and the PhD in Electrical Engineering from Cornell and he joined the University of Wisconsin-Madison faculty in 1989. His industrial experience included writing a general simulation of switching power supplies and his current interests include voltage collapse in electric power systems and applications of nonlinear dynamics and bifurcation theory.

**Willis F. Long** (M'69, F'89) received his B.Sc. and M.Sc. in Engr. Physics and EE from the Univ. of Toledo, and the PhD in EE from the Univ. of Wisconsin-Madison in 1970. He was a technical staff member at Hughes Research Labs. and Director of ASEA Power Systems Center, New Berlin, WI. Since 1973 he has been on the faculty of the Univ. of Wisconsin-Madison. Dr. Long's research interests are in the analysis and simulation of HVDC transmission systems.